J Mater Sci: Mater Med (2015) 26:17
DOI 10.1007/s10856-014-5333-y

Structural and biological evaluation of lignin addition to simple and silver-doped hydroxyapatite thin films synthesized by matrix-assisted pulsed laser evaporation

A. Janković · S. Eraković · C. Ristoscu · N. Mihailescu (Serban) · L. Duta · A. Visan · G. E. Stan · A. C. Popa · M. A. Husanu · C. R. Luculescu · V. V. Srdić · Dj. Janaćković · V. Mišković-Stanković · C. Bleotu · M. C. Chifiriuc · I. N. Mihailescu

Received: 27 February 2014 / Accepted: 28 July 2014 / Published online: 13 January 2015
© Springer Science+Business Media New York 2014

Abstract We report on thin film deposition by matrix-assisted pulsed laser evaporation of simple hydroxyapatite (HA) or silver (Ag) doped HA combined with the natural biopolymer organosolv lignin (Lig) (Ag:HA–Lig). Solid cryogenic target of aqueous dispersions of Ag:HA–Lig composite and its counterpart without silver (HA–Lig) were prepared for evaporation using a KrF* excimer laser source. The expulsed material was assembled onto TiO_2/Ti substrata or silicon wafers and subjected to physical–chemical investigations. Smooth, uniform films adherent to substratum were observed. The chemical analyses confirmed the presence of the HA components, but also evidenced traces of Ag and Lig. Deposited HA was Ca deficient, which is indicative of a film with increased solubility. Recorded X-ray Diffraction patterns were characteristic for amorphous films. Lig presence in thin films was undoubtedly proved by both X-ray Photoelectron and Fourier Transform Infra-Red Spectroscopy analyses. The microbiological evaluation showed that the newly assembled surfaces exhibited an inhibitory activity both on the initial steps of biofilm forming, and on mature bacterial and fungal biofilm development. The intensity of the anti-biofilm activity was positively influenced by the presence of the Lig and/or Ag, in the case of *Staphylococcus aureus*, *Pseudomonas aeruginosa* and *Candida famata* biofilms. The obtained surfaces exhibited a low cytotoxicity toward human mesenchymal stem cells, being therefore promising candidates for fabricating implantable biomaterials with increased biocompatibility and resistance to microbial colonization and further biofilm development.

1 Introduction

Titanium (Ti) is widely used as an implantable biomaterial for medical devices like dental implants, fracture fixations and joint replacements [1, 2], due to its high strength, toughness, and durability. However, Ti requires an appropriate surface biofunctionalization to increase hard and/or soft tissue compatibility and to exhibit antimicrobial

A. Janković · S. Eraković
Innovation Center, Faculty of Technology and Metallurgy, University of Belgrade, 11000 Belgrade, Serbia

C. Ristoscu · N. Mihailescu (Serban) · L. Duta · A. Visan · C. R. Luculescu · I. N. Mihailescu (✉)
National Institute for Lasers, Plasma and Radiation Physics, 077125 Magurele, Ilfov, Romania
e-mail: ion.mihailescu@inflpr.ro

G. E. Stan · A. C. Popa · M. A. Husanu
National Institute of Materials Physics, 077125 Magurele, Ilfov, Romania

A. C. Popa
Army Centre for Medical Research, 020012 Bucharest, Romania

V. V. Srdić
Department of Materials Engineering Faculty of Technology, University of Novi Sad, 21000 Novi Sad, Serbia

Dj. Janaćković · V. Mišković-Stanković
Faculty of Technology and Metallurgy, University of Belgrade, 11000 Belgrade, Serbia

C. Bleotu
Stefan S. Nicolau Institute of Virology, 030304 Bucharest, Romania

M. C. Chifiriuc
Department of Microbiology, Faculty of Biology, University of Bucharest, 060101 Bucharest, Romania

properties for the inhibition of biofilm formation. Biofilm represents a microbial community that irreversibly attaches to a host surface, being protected by a self-secreted extracellular polymeric matrix and other complex mechanisms from the action of antibiotics, disinfectants and host immune effectors.

Despite their frequent presence as commensal bacteria on the human skin and mucous surfaces, staphylococci are the most frequent causes of biofilm-associated infections, especially in intensive care patients. Studies have shown that *Staphylococcus aureus* could form static biofilms on different modified Ti surfaces. The Ti coating with sodium hyaluronate thin films [3], the hydrophobic and superhydrophobic surfaces resulting from Ti surface modification by TiO_2 nanotube arrays or pure Ti treated with 1H, 1H, 2H, 2H-perfluorooctyl-triethoxysilane [4], as well as Ag nanoparticle-modified Ti [2] proved to be efficient in preventing *S. aureus* biofilm-associated infections.

Pseudomonas aeruginosa is an opportunistic human pathogen causing a wide range of infections, from wound infections to lung diseases in patients with cystic fibrosis and medical device-associated infections [5]. Studies have shown that the sol–gel TiO_2 with Ag or Degussa TiO_2 with Ag attenuate *P. aeruginosa* adherence and growth [6].

Fungi most commonly related to biofilm-associated infections belong to the genus *Candida,* being usually connected with indwelling medical devices. The development and characterization of *C. albicans* biofilms formed on bioprosthetic materials have been intensively investigated [7]. Malm et al. [8] studied *C. famata* biofilm development on glass slides by microscopic examination. It was observed that after 24 h of incubation, *C. famata* biofilm is still growing, and after 72 h it reaches the stage of a mature biofilm, accompanied by changes in morphological reorganization.

Although Ti does not possess intrinsic antifungal properties, TiO_2 can act as a photocatalyst for the decomposition of organic compounds under UV irradiation, reducing the viability of *C. albicans* [9, 10]. Ti-coated silicone was thought to prevent *Candida* biofilm formation on voice prostheses by increasing the smoothness of the material surface [11].

Due to the dramatic increase of traumatic, pathological or surgical injury cases that require hard-tissue implants, many techniques for Ti surface modification, such as coating with hydroxyapatite [HA, $Ca_{10}(PO_4)_6(OH)_2$], have been developed, some of them being already commercialized [12, 13]. HA is an excellent biocompatible material, and it is largely used nowadays in medicine in all forms (bulk, coating, emulsion) [14], due to its chemical and structural similarities to the mineral part of the human bone tissue.

Doping HA with antimicrobial agents, especially with silver (Ag) ions, is a promising approach to address the difficult problem of microbial biofilm-associated infections on medical prostheses [15]. As biofilms are the most common mode of bacterial growth and lead consistently to clinical infections (up to 80 %), especially because of their high antibiotic resistance, there is a stringent need for new and efficient implant functionalization solutions. Biofilms on indwelling medical devices result in significant morbidity and mortality and have a substantial impact on healthcare systems worldwide [16]. Biomaterial-associated infection incidence is increasing proportionally to the number of people gaining access to medical device technologies worldwide, but also due to the emerging microbial resistance to current antibiotics [17]. The clinical experience showed that Ti devices are frequently colonized by microbial strains and the subsequent biofilm formation represents a huge complication in implant surgery [18].

Recent research advances in understanding the interaction between microbial biofilms and Ti surface contributed to the development of novel preventive strategies to control medical device-related infections. The focus is on obtaining improved biomaterials with increased resistance to microbial colonization via surface physical–chemical modifications. Today, Ag and Ag nanoparticles are mostly used in a wide range of applications: healthcare, textile, food, hard surface material industry or domiciliary applications [18, 19]. Ag ions possess strong antimicrobial properties, which, correlated with no immediate and serious risk for human health, have led to an extensive use of Ag-based products in many biomedical applications [18, 19].

Lignin (Lig) is a complex, amorphous organic polymer found in plant tissues, usually bound to cellulose. Phenylpropane units in Lig are cross-linked to each other by various chemical bonds. Lig is a well-known and important source of natural antimicrobial and antifungal compounds [20].

We have previously reported on composite HA–Lig materials that could be used as biomedical coatings [21, 22] exhibiting enhanced bioactivity and osteoconductivity. The novel concept of engaging natural biopolymer Lig in composite coatings was studied—so far by electrophoretic deposition only [23, 24]. However, an unaltered incorporation of this specific organic material could provide a composite with enhanced stability and improved interconnected structure, which will increase the coating cohesion.

Matrix-assisted pulsed laser evaporation (MAPLE) technique is derived from Pulsed Laser Deposition (PLD), developed for controlled assembly of biopolymer thin films [25, 26]. The method is based upon a cryogenic approach which secures the transfer of organic macromolecular materials. The key components are dissolved or suspended in an appropriate volatile solvent, which is flash-frozen to form a «target». Due to the low concentration of biomolecules, the laser photons mostly react with the frozen matrix (solvent), which vaporizes and gets pumped out of

the deposition chamber. Thus, organic molecules of the frozen target can get transferred undamaged and not degraded to the substratum [27–29].

In a recent paper, we have demonstrated the positive role of the Ti surface modification by arrays of TiO_2 nanotubes on the biocompatible and antifungal response of top HA layers deposited by PLD [30]. In the present research, we aimed to obtain biomimetic ceramic-polymer composite coatings for medical Ti implants modified with 100 nm diameter TiO_2 nanotubes (fabricated by anodization of Ti plates) by employing MAPLE as fabrication method. Composite HA–Lig and Ag doped HA–Lig were transferred by this technique, their structure and composition were assessed, as well as their cytotoxicity against human Wharton's Jelly-derived mesenchymal stromal cells (WJ-MSCs) and antimicrobial efficiency against Gram-positive (*S. aureus* ATCC 6533), Gram-negative (*P. aeruginosa* ATCC 27853) bacterial and fungal (*C. famata* 30) strains.

The main purpose of the microbiological assay was to evaluate the anti-biofilm efficiency of thin films of simple hydroxyapatite (HA) or silver (Ag) doped HA combined with the natural biopolymer organosolv (Lig) (Ag:HA–Lig), deposited by MAPLE.

2 Experimental

2.1 Preparation of Ti substrata

Pure Ti foils ($20 \times 10 \times 0.25$) mm^3 in size and 99.7 % purity (Sigma Aldrich) were used as substrata for the growth of arrays of TiO_2 nanotubes by anodization technique described in Ref. 30. As prepared, TiO_2/Ti substrata were degreased in acetone, then in ethanol, each for 30 min in ultrasonic bath and finally kept in ethanol until deposition. Just before their introduction into the reaction chamber, the substrata were rinsed with deionized water and jet-dried with N_2.

2.2 Preparation of HA and Ag/HA powders

For the preparation of HA powder with and without Ag we used a modified chemical precipitation method [21]. Calcium oxide, synthesized by aerobic calcination of $CaCO_3$ for 5 h at 1000 °C, was placed in a reaction vessel with Ag nitrate ($AgNO_3$), in the case of Ag:HA, and phosphoric acid. The reaction was conducted in a step-wise manner. A stoichiometric amount of the resulting calcium oxide was mixed and stirred in distilled water for 10 min. Afterwards, $AgNO_3$ solution was added to the suspension, to reach a final concentration of Ag ion of (0.6 ± 0.1) wt%. Finally, phosphoric acid was added drop-wise to the suspension in order to obtain HA or Ag/HA powder, $Ca_{9.95}Ag_{0.05}(PO_4)_6(OH)_2$. After the required quantity of phosphoric acid was introduced, the pH reached a value of 7.4–7.6. The obtained suspension was preheated to (94 ± 1) °C for 30 min and stirred for another 30 min. After sedimentation, the upper clear solution layer was decanted from precipitate. The suspension was then spray-dried at (120 ± 5) °C into granulated powder.

2.3 Cryogenic target preparation and mounting

Organosolv Lig (extracted by the Alcell process) was used for preparing organic–inorganic composite targets.

Solutions consisting of HA or Ag:HA powders (10 % w/v) and Lig (1 % w/v) dissolved in distilled water were homogenized by rapid vortexing and flash frozen in a liquid nitrogen cooled copper container. The container with the obtained frozen target (HA–Lig or Ag:HA–Lig pastilles) was then mounted on a cryogenic holder inside the deposition chamber and rotated at 10 rpm to avoid local overheating and excess ablation during multipulse laser irradiation. The holder was submerged in liquid nitrogen flow in order to keep the targets frozen during the experiments.

2.4 MAPLE experiment

HA–Lig and Ag:HA–Lig composite coatings deposition was performed at room temperature in a pressure of 6.5 Pa onto TiO_2/Ti substrata. The target-to-substratum separation distance was 35 mm. A pulsed KrF* excimer laser source ($\lambda = 248$ nm, $\tau_{FWHM} \leq 25$ ns) operating at 10 Hz was used for target evaporation. The laser beam was incident onto the target surface at 45°. The spot size was of 25 mm^2. A total of 35,000 pulses with an incident laser fluence of 0.7 Jcm^{-2} were applied for the deposition of each structure. It is important to note that this fluence level is about five times lower than in conventional PLD of inorganic materials, as a supplementary precaution adopted in MAPLE to protect Lig molecules against extensive laser beam irradiation. Twin samples were deposited on <111> single-crystalline Si wafers.

2.5 Morphological, structural and compositional characterization

The surface morphology of the deposited films was investigated by scanning electron microscopy (SEM) with a *Carl Zeiss EVO 50 XVP* instrument, operated at 30 kV acceleration voltage and 10 μA beam current, under secondary electron mode. No conductive coating was applied onto film surface. Cross-sectional SEM images were recorded on HA–Lig and Ag:HA–Lig films deposited on Si wafers in order to evaluate their thickness.

Composition analysis was performed by energy dispersive spectroscopy (EDS), with a *SiLi EDAX Inc.* detector, operated at 20 kV. The measurements were conducted in duplicate, on different, relatively large regions of (250 × 250) μm^2.

The crystalline status of the MAPLE thin films was evaluated by Grazing Incidence X-ray diffraction (GIXRD) using a *Bruker D8 Advance diffractometer*, in parallel beam setting, equipped with a Cu target X-ray tube. The incidence angle was set at 2°, and the scattered intensity was scanned in the range 20–50° (2θ), with a step size of 0.04°, and 50 s per step.

X-ray photoelectron spectroscopy (XPS) analysis was performed to assess the Lig transfer. The XPS measurements were conducted in a *SPECS* dedicated surface science facility, keeping the base pressure during measurements below 10^{-8} Pa. The spectra were recorded using the Al $K_{\alpha 1}$ monochromatized radiation (E = 1486.74 eV) in an analysis chamber equipped with a 150 mm hemispherical electron energy analyzer (Phoibos). Fixed analyzer transmission mode was operated with pass energy of 20 eV and step energy of 0.05 eV. The estimated combined (source + analyzer) resolution was about (0.75 ± 0.025) eV. During the XPS measurements, a flood gun operating at 1 eV acceleration energy and 100 μA electron current was used in order to achieve sample neutralization.

The short-range order analysis and the detection of the functional groups present in the MAPLE films was carried out by Fourier transform infra-red (FTIR) spectroscopy in attenuated total reflection (ATR) mode using a *Perkin Elmer BX Spectrum-Pike* spectrometer equipped with a *Pike-MIRacle* ATR diamond head of 1.8 mm in diameter. The spectra were collected over a range of (4000–550) cm^{-1} by recording 150 individual scans at 4 cm^{-1} resolution. During acquisition, the spectrometer chamber was continuously purged with nitrogen to maintain a dry environment.

2.6 Biological assays

2.6.1 Cytotoxicity assay

The biological compatibility of the MAPLE composite coatings was assessed by cultivating human Wharton's Jelly-derived Mesenchymal Stromal Cells (WJ-MSCs) on their surface. Quantification of cells was performed using propidium iodide (PI). To this purpose, the obtained specimens were sterilized by UV irradiation and placed in 35 mm diameter Petri dishes. In each Petri dish 3×10^5 mesenchymal cells were added. The monolayer morphology was evaluated after 24 h, by fixing the cells with 70 % alcohol and staining the monolayer with 5 μg/mL PI. The stained specimens have been examined and photographed in fluorescent microscopy [31].

2.6.2 Microbial biofilm assay

The microbial adherence ability and biofilm development on the functionalized surfaces have been investigated by two culture-based methods, using Gram-positive (*S. aureus* ATCC 6533), Gram-negative (*P. aeruginosa* ATCC 27853) bacterial and fungal (*C. famata* 30) strains. The specimens (composite coatings and pure HA controls) of the same size have been distributed in the multi-well plastic plates, and exposed to UV sterilization for 30 min. The pure HA controls have been synthesized by PLD in optimized conditions [30]. All experiments were performed in duplicate. Thereafter, the liquid culture medium (nutrient broth) was added over the slide specimens. Each well was inoculated with a microbial inoculum with a density corresponding to 0.5 MacFarland density prepared in sterile saline. Each microbial strain was inoculated in two wells containing the same specimen. Thus prepared samples were incubated at 37 °C, in order to allow microbial strains to multiply and adhere to the deposited Ti plates, distributed in each well.

After 24, 48 and 72 h, respectively, the specimens were extracted, washed three times in sterile saline, in order to remove the non-adherent bacteria and moved in sterile plastic wells. Fresh culture medium was thereafter added and the multi-well plates were further incubated at 37 °C for 24 h. This point forward, the specimens have been treated differently, in order to assess:

a) *The total biofilm (viable and dead) cells*
For the purpose of our assay, after incubation, the density of the obtained cultures recovered after the multiplication of microbial cells adhered to the tested substrata was measured at 600 nm.

b) *The viable cells embedded into the biofilms developed on different specimens.*
Ten-fold dilutions were prepared from the cultures recovered after the multiplication of microbial cells adhered to the tested substrata in order to count the Colony Forming Units (CFU) and to assess the viable cell counts (VCCs) of the respective cultures. For this purpose, the adhered cells have been removed from samples by vortexing and brief sonication. Serial dilutions ranging from 10^{-1} to 10^{-30} of the obtained inocula have been spotted on Muller-Hinton agar, incubated for 24 h at 37 °C and assessed for VCCs. An amount of 5 μl of the chosen dilution was spotted in duplicates on the solid medium. The resulting colonies have been numbered and the average value was submitted to dilution and volume correction. The

final value was expressed in CFU/mL. Performing the assay in this manner, we were able to assess the influence of different tested substrata on the adherence and the dynamics of microbial biofilm development by selected microbial strains.

3 Results and discussion

3.1 SEM–EDS

Typical top-view SEM images of the HA–Lig and Ag:HA–Lig films are displayed in Fig. 1. MAPLE deposition resulted in rather smooth films with a homogenous and pore-free microstructure, without particular morphological features. Rough surface of the films was reported starting from the same nanohydroxyapatite powder composite with Lig, when using the electrophoretic deposition [21]. As an important note, no remarkable morphological differences have been evidenced between the HA–Lig and Ag:HA–Lig films.

The cross-sectional SEM images collected in case of films deposited onto Si wafers, revealed the compact look of these MAPLE coatings with good adhesion to the substratum. A thickness of $\sim 180 \pm 10$ nm has been estimated based upon the cross-sectional SEM analyses. A typical cross-SEM image of the Ag:HA–Lig film grown on a silicon wafer is visible in Fig. 1b-inset.

The qualitative EDS analyses (data not shown) revealed the high purity of films and indicated the presence of all elements of HA, along with carbon content for both types of films, suggesting the incorporation of Lig. Small traces of Ag have been detected in the case of Ag:HA–Lig films. The quantitative EDS estimation indicated the synthesis of a calcium deficient HA phase, as the atomic Ca/P ratio was slightly altered during the ablation process down to a value of ~ 1.33 (inferior to 1.67 theoretical Ca/P ratio, characteristic to stoichiometric HA). Such a deviation could be associated with Ca/P ratio dependence on substratum temperature and laser incident fluence [25, 28, 30]. Small traces of Ag (~ 0.57 wt%) have been detected in the case of Ag:HA–Lig films. However, because of the low accuracy of the EDS technique, this value should be considered as a rough approximation only.

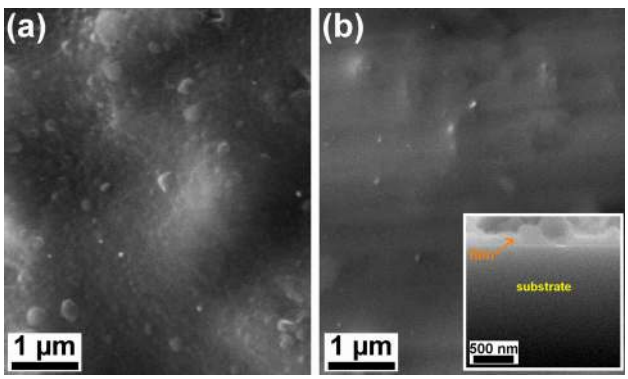

Fig. 1 *Top-view* SEM micrographs of the HA–Lig (**a**) and Ag:HA–Lig (**b**) films deposited onto TiO_2/Ti substrata by MAPLE. Inset: cross-view SEM micrograph of Ag:HA–Lig film deposited onto silicon wafer

3.2 XRD

The GIXRD patterns revealed the Ti substratum maxima only, suggesting that the TiO_2 nanotubes, as well as the HA–Lig and the Ag:HA–Lig coatings synthesized by MAPLE were amorphous within the experimental sensitivity limit of the apparatus. A typical GIXRD pattern (for the Ag:HA/TiO_2/Ti film) is presented in Fig. 2. For comparison, the reference files of hydroxyapatite (ICDD: 00-009-0432), anatase (ICDD: 00-021-1272) and rutile ((ICDD: 00-021-1276) are superimposed on the graph.

3.3 XPS

The XPS spectra were recorded for the pure HA, HA–Lig and Ag:HA–Lig films.

As known, charging effects may arise during measurements, resulting in an apparent shift of core-level XPS lines [32]. Mitigating this effect usually involves using a flood-gun corroborated to overall shift of all lines with values that correlate to C1 s line at 284.5 eV, considered as standard. In our case such calibration is difficult since C1 s band has a complex structure, featured by several components. In fact, their assignment is essential in identifying the Lig signature in the XPS spectrum.

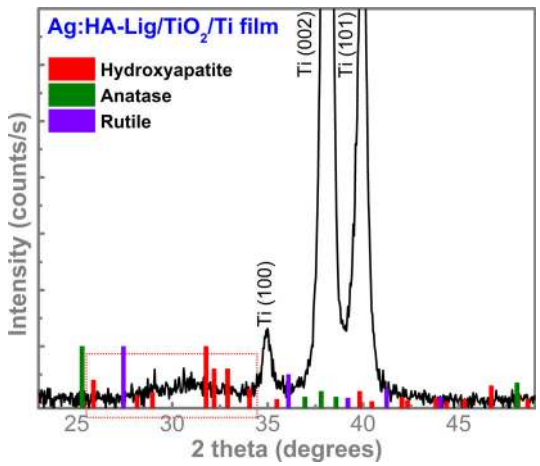

Fig. 2 Typical GIXRD pattern of a Ag:HA–Lig/TiO_2/Ti film deposited by MAPLE

In order to identify the contamination-associated component, a 30 s Ar^+ sputtering was performed at accelerating voltage of 3 kV resulting in an ion current of $\sim 15 \times 10^{-6}$ A. Assuming that every incoming ion pulls-out a surface atom, one estimates that in 30 s we remove 2 nm approximately from the surface layer. Based on this assumption, we expect that the signature provided by C1 s spectrum entirely belongs to pure HA, HA–Lig and Ag:HA–Lig composite films, free of any contamination. Consequently, C-bonded carbon line was identified as the component with the most evident intensity drop-off, and it was kept at 284.5 eV and used as calibration line.

The presence of Lig was demonstrated in both HA–Lig and in the more complicated case of Ag:HA–Lig. For discussion, we therefore focused on a comparison of the XPS data between pure HA and Ag:HA–Lig coatings. The intensity variation of the C1 s XPS components after the sputtering cycle is given for the two cases (Fig. 3). The Lig signature was revealed to be dispersed in the HA matrix, as evidenced by a massive increase of the C-bonded carbon signature, accompanied by a slight increase of the component associated with oxygen-bonded C or oxygen-containing radicals (Table 1).

The indisputable proof that the Lig has been effectively transferred into the HA composite film would consist in determining the experimental stoichiometry fraction xC:yO from the XPS data considering the addition of 10 % Lig into the HA matrix.

From the experimental stoichiometry inferred for the pure HA case aC:bO and that of the HA–Lig composite $0.9[a\text{C}:b\text{O}] + 0.1[x\text{C}:y\text{O}]$, the values obtained were $x = 11$, $y = 4.4$. These values closely correspond to the Lig theoretic stoichiometry of the three monolignols ($C_9H_{10}O_2$/$C_{10}H_{12}O_3$/$C_{11}H_{14}O_4$) (Fig. 4) which lead to Lig formation by polymerization. As a crosscheck and as suggested in previous studies [33–35], we have also calculated the theoretical stoichiometry of the dopant using the integral amplitudes of the C1 s and O1 s peaks. Comparable results have been obtained, i.e. $x = 11$, $y = 3.75$. These findings validate the experimental results.

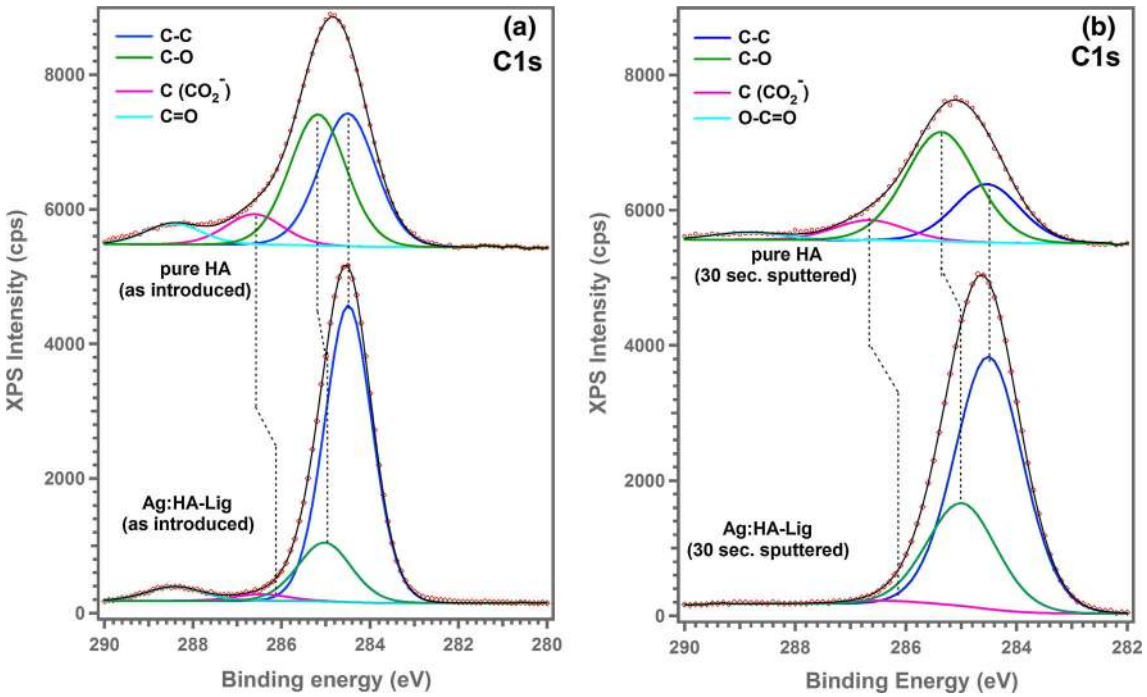

Fig. 3 C 1 s core level high resolution XPS spectra of pure HA (**a**) and Ag:HA–Lig (**b**) films

Table 1 C 1 s XPS core level sub-components areas

	% C for "as-introduced" samples				% C for 30 s sputtered samples			
	C–C/C–H	C–OH/C–OR	C = O/HO–C–OR	C = O	C–C/C–H	C–OH/C–OR	C = O/HO–C–OR	C = O
Pure HA	41.86	41.79	9.70	6.65	28.33	57.37	10.35	3.95
Ag:HA–Lig	76.7	17.08	1.91	4.31	70.42	27.10	2.48	–

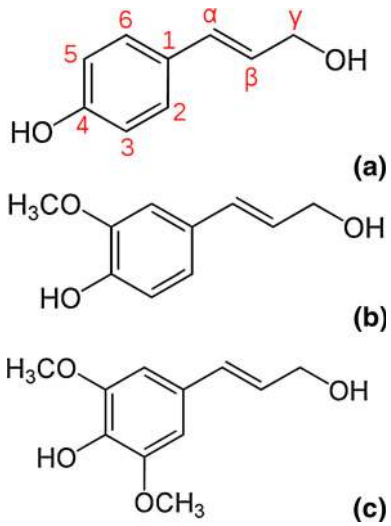

Fig. 4 Theoretical stoichiometry and chemical formulas of the three monolignols: (**a**) hydroxyphenyl ($C_9H_{10}O_2$), (**b**) guaiacyl ($C_{10}H_{12}O_3$) and (**c**) syringyl ($C_{11}H_{14}O_4$) [36]

3.4 ATR-FTIR

FTIR spectroscopy was applied for identifying the functional groups and the degree of short-range ordering in the deposited films. Emphasis was put on identifying the distinct chemical bonds of Lig and the degree of macromolecule decomposition during MAPLE transfer, if any.

The ATR-FTIR spectra of the original Lig powder, pure HA powder, and pure HA and Ag:HA–Lig films (deposited under optimized conditions) are shown comparatively in Fig. 5. The assignment for the IR vibration bands is given in Table 2.

In the fingerprint region (1800–550 cm^{-1}), Lig powder exhibits an intricate spectrum with numerous sharp and discrete absorption bands due to its main molecular components (Table 2). HA–Lig and Ag:HA–Lig coatings had similar envelopes dominated by the typical vibration bands of HA [37]: the ν_4 symmetric bending, ν_1 symmetric and ν_3 asymmetric stretching modes of phosphate groups, along with the libration mode of structural OH (see Table 2). Because of the complex composition of Ag:HA–Lig coatings, we chose to present in Fig. 5e the IR spectrum of this film only.

In the (1200–550) cm^{-1} wave number region the prominent HA bands are superimposed to some of the Lig bands, partly obscuring them. Moreover, in the (890–660) cm^{-1} region, the intense band of the Ti–O and Ti–O–Ti skeletal vibrations is brought in by the underlayer of TiO_2 nanotubes [38]. However, the Lig contribution can be hinted by a more complex shape of the IR envelope in the case of Ag:HA–Lig composite film (Fig. 5e) with respect to the pure HA film and powder spectra (Fig. 5c, d).

The undeniable evidence of the Lig macromolecule transfer is revealed by the distinct bands of Lig visible in the (1800–1200) cm^{-1} (Fig. 5a, e, inset) and the (3100–1200) cm^{-1} (Fig. 5b, f) wave number regions [39–41]. The presence, in these specific spectral regions, of all Lig vibration bands, suggests that the Lig material is not altered during the MAPLE transfer, the slight shifts being induced rather by the molecular interactions with the HA matrix than by its degradation.

The broader IR spectrum in the case of Ag:HA–Lig composite film also indicates that a short-range ordering alteration occurred as a consequence of intermolecular interactions between the HA film matrix and the Lig components. Differences in the absorbance values and shape of the bands were also detected in the infrared spectra, pleading as well for intimate structural modification induced by the Lig embedment in the HA film matrix.

The stretching modes of guaiacyl (G) and syringyl (S), archetypal for Lig, were evidenced in the composite films at the 1205 (G), 1283 (G), and 1320 cm^{-1} (S), respectively. The guaiacyl IR bands are dominant which suggests that a larger amount of G units is present in the film. Higher G/S ratios could increase cross-linking of the Lig molecules [40] dispersed in the entire HA matrix, and thus, could contribute to the augmentation of the mechanical properties of the film and a more durable composite material.

3.5 Effect of the prepared samples on WJ-MSCs viability

Stem cells and progenitor cells are promising candidates for the development of efficient therapeutic and regenerative strategies, with a large spectrum of clinical applications, including biomaterials and tissue engineering [45]. MSCs are adult stem cells able to differentiate into a variety of cell types in vitro, but also to engraft in vivo [46, 47]. We therefore decided to use MSC for our in vitro cytotoxicity tests, with the conviction that the results would be a solid foundation for future in vivo biocompatibility studies of the MAPLE coatings.

We would like to emphasize that no significant changes were observed in the morphology of WJ-MSCs, when grown on the surface of the tested materials. The experiments have shown that the MAPLE composite coatings exhibited no toxicity towards human cells and allowed a sustained growth of WJ-MSCs.

It appears that the presence of Lig improves the biocompatibility of the HA coated TiO_2/Ti, by promoting the growth of adhered cells, clearly supporting the suitability of our composites for developing future biomaterials with increased biocompatibility (Fig. 6).

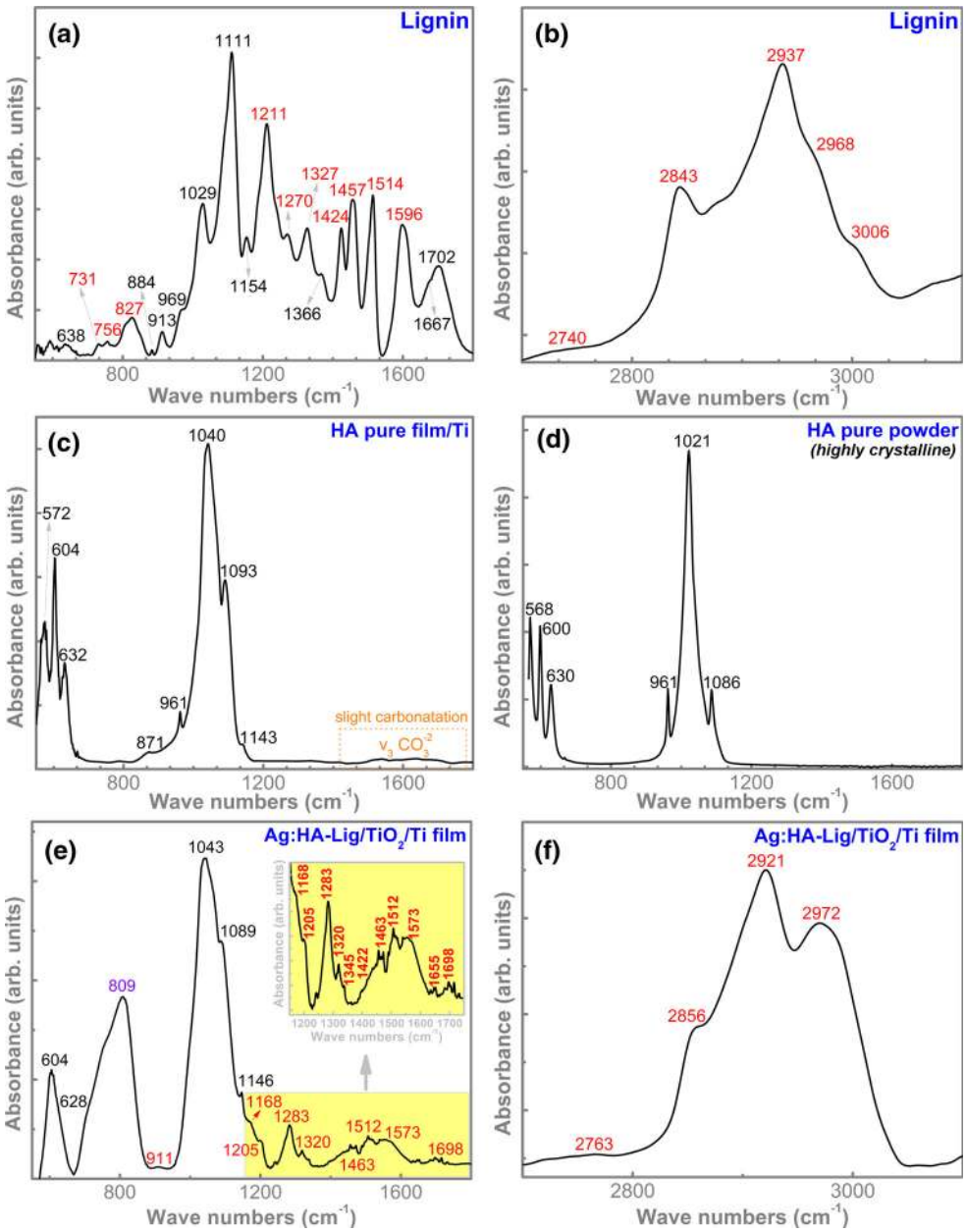

Fig. 5 ATR-FTIR spectra of Lig powder (**a**, **b**), pure HA film (**c**), pure HA powder (Sigma-Aldrich) (**d**) and Ag:HA–Lig film (**e**, **f**) in the spectral regions: 1800–550 cm^{-1} (**a**, **c**, **d**, **e**) and 3100–2700 cm^{-1} (**b**, **f**)

3.6 Microbial assay results

Our initial hypothesis was that adding Lig to HA-films doped with Ag ions would yield a material with improved antimicrobial properties. To test this hypothesis, we have examined the anti-biofilm efficiency of the bioactive composite coatings, by using two well-established microbiological assays. One is based upon the assessment of VCCs, whilst the second resorts to bacterial culture density measurements, for the quantification of total microbial biofilm developed on the materials obtained at different time intervals, i.e. 24, 48 and 72 h, respectively. These two approaches could provide complementary information regarding the number of viable cells embedded in the biofilm (viable cell counts) as well as the density of microbial biofilm (comprised of both viable or dead cells and the biofilm matrix).

The temporal dynamics of biofilms formed by microbial species, either fungi or bacteria are different, as it is their resistance to various antimicrobial agents [48, 49]. However, research performed in many biofilm-forming organisms has revealed that the development of a biofilm is a two-step process involving an initial attachment and a subsequent maturation phase, which are physiologically different from each other and require phase-specific factors. A final dispersal phase involves the detachment of

Table 2 Assignment of ATR-FTIR vibration bands for the lignin powder, pure synthetic HA powder (Sigma-Aldrich), pure HA film, and Ag:HA–Lig composite film

Observed IR bands (cm^{-1})				Bands' assignment
Pure Lig	Pure HA powder	Pure HA film	Ag:HA–Lig film	
–	568	572	604	Asymmetric bending (ν_4) of **$(PO_4)^{3-}$ groups** [37]
–	600	604		Asymmetric bending (ν_4) of **$(PO_4)^{3-}$ groups** [37]
–	630	632	628	Librational mode of **$(OH)^-$ groups** [37]
638	–	–	–	**C–OH** out-of-plane bending [42]
731	–	–	–	**C–H** bonds on the benzene rings [43]
756	–	–	749	Asymmetric bending of **HCCH groups** [39]
–	–	–	809	**Ti–O** vibrations [38]
827	–	–	–	**C–H** out-of-plane in position 2 and 6 of **syringyl** (**S**) and in all positions **guaiacyl** (**G**) **units** [39, 40]
–	–	871	–	Vibrations of **$(HPO_4)^{2-}$ ions** [37]
884	–	–	–	**C–H** deformation vibration of **cellulose** [39]
913	–	–	911	**C–H** bending of **S units** [39]
–	961	961	942	Symmetric stretching (ν_1) of **$(PO_4)^{3-}$** groups [37]
969	–	–	–	**=CH** out-of-plane deformation [39, 41]
1029	–	–	–	**C–O** stretching of **cellulose** [39, 41]
–	1021	1040	1043	Asymmetric stretching (ν_3) of **$(PO_4)^{3-}$** groups [37]
–	1086	1093	1089	Asymmetric stretching (ν_3) of **$(PO_4)^{3-}$** groups [37]
1111	–	–	–	**C=O** stretching [41]
–	–	1143	1146	Vibrations of **$(HPO_4)^{2-}$ ions** [37]
1154	–	–	1168	**C–O–C** asymetric stretching in cellulose [39, 41]
1211	–	–	1205	**C–C**, **C–O** and **C=O** stretching of **G units** [39, 40]
1270	–	–	1283	**C–O** stretching of **G units** [39, 41]
1327	–	–	1320	**C–O** stretching of **S units** [39, 41]
1366	–	–	1345	**C–H** symmetric bending in cellulose [40, 41]
1424	–	–	1422	**C–H** in plane bending in Lig [39, 41]
1457	–	–	1463	**C–H** bending of **methyl** and **methylene groups** [39, 41]
1514	–	–	1512	**C = C stretching of the aromatic ring** (**G**) [40, 41]
1596	–	–	1573	**C=C stretching of the aromatic ring** (**S**) [41]
1667	–	–	1655	**C=O** stretching in conjugated p-subst. **aryl ketones** [40]
1702	–	–	1698	**C=O** stretching in unconjugated **aldehyde**, **ketone**, **carbonyls** or **ester** groups [39, 40]
2740	–	–	2763	Aldehyde **C–H** stretch [39, 41]
2843	–	–	2856	Asymmetric **CH** stretching in aromatic **methoxyl** groups and in **methyl** and **methylene** groups of side chains [41]
2937	–	–	2921	Symmetric **CH** stretching in aromatic methoxyl groups and in methyl and methylene groups of side chains [41]
2968	–	–	2972	sp^3 hybridized **C–H** [44]
3006	–	–	–	sp^2 hybridized **C–H** [44]

single cells or cell clusters promoting the bacterial dissemination [50]. In the maturation phase, bacterial cells proliferate and produce an extracellular matrix consisting of several secreted polymers, such as exopolysaccharides, teichoic acids and specific proteins, as well as DNA originating from the lysed bacteria [51].

The observed dynamics of *S. aureus* biofilm formation varied depending on the tested specimen.

The biofilm developed on the pure HA coating control specimen showed a growth peak at 48 h, the number of viable bacterial cells recovered at 48 h remaining practically constant at 72 h (Fig. 7a).

At 24 h, the number of viable cells harvested from the HA–Lig and Ag:HA–Lig samples slightly increased with respect to control, by 3–4 logs (Fig. 7a). At 48 h, the number of viable cells embedded in the biofilm developed

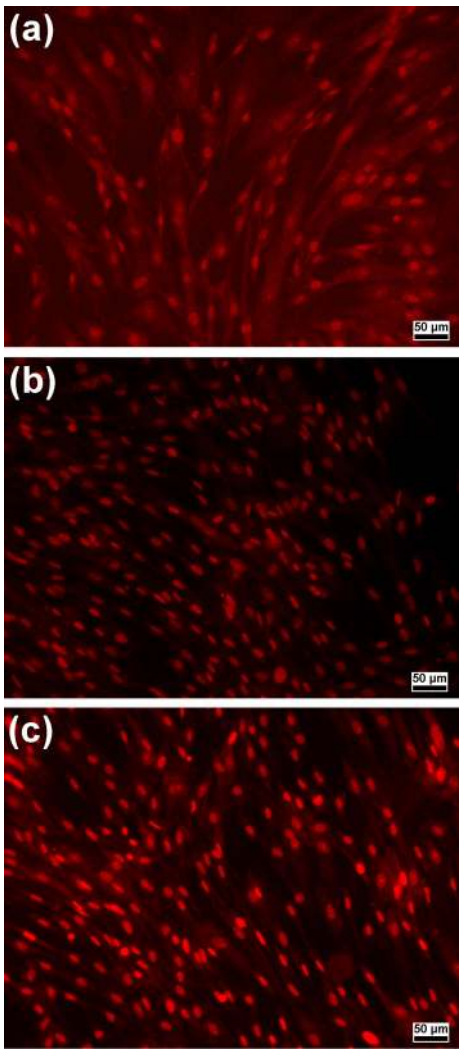

Fig. 6 Fluorescence microscopy images of nuclei of WJ-MSCs grown on different substrata: pure HA (**a**); HA–Lig (**b**); and Ag:HA–Lig (**c**) films. Magnification: ×200

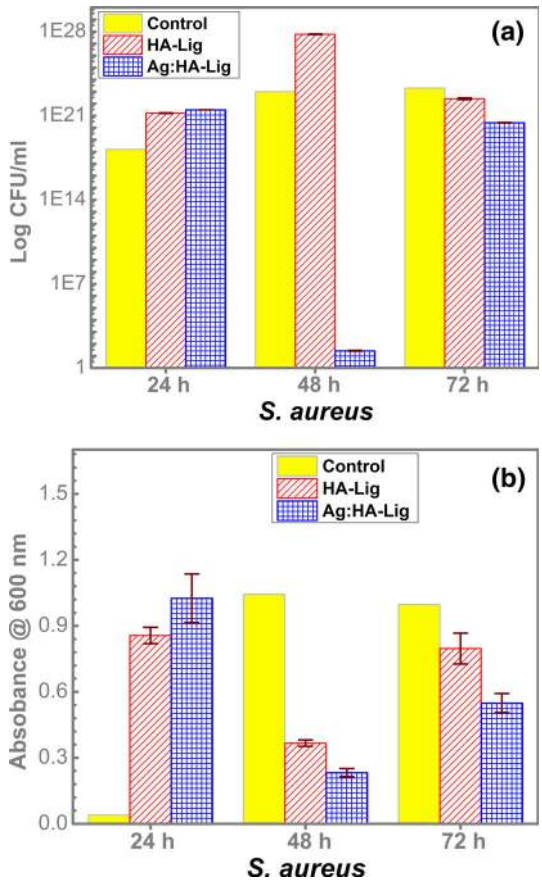

Fig. 7 (**a**) Number of *S. aureus* viable cells recovered from the biofilms growing on the tested specimens after 24, 48 and 72 h, respectively; (**b**) Absorbance values at 600 nm of the *S. aureus* bacterial biofilm developed on the tested specimens after 24, 48 and 72 h, respectively

on the HA–Lig still showed increased values exceeding by 4.5 logs the number of VCCs obtained for the HA control, whilst for the Ag:HA–Lig coating was drastically lowered (the recovered VCCs being by 20 logs less than control) (Fig. 7a), suggesting the gradual and prolonged release of silver ions from the organic–inorganic composite coatings, that interfere with the staphylococcal mature biofilm development. The HA–Lig and Ag:HA–Lig specimens exhibited a similar anti-biofilm activity against the 72 h biofilms (reducing by 1.5–2.5 logs the VCCs as compared to control) and supporting the hypothesis that Lig improves the implants long-time resistance to staphylococcal colonization. However, even though a more significant decrease of VCCs was observed as compared to control, the increased number of VCCs developed at 72 h, as compared to 24 and 48 h, is pleading for the role of silver ions in the prevention of microbial adherence and for the fact that silver ions are mostly released from the coating in the first 48 h of incubation.

The density of the microbial cultures resulting from the multiplication of 24 h biofilm embedded cells and measured at 600 nm proved to be much higher than for pure HA coating control (Fig. 7b). Conversely, in the case of the 48 and 72 h biofilms, the microbial culture density was decreasing in the presence of composite MAPLE coatings compared to the control. Thus, as an effect of the Lig introduction, the hydroxyapatite composite coating (HA–Lig) gained the ability to prevent the development of *S. aureus* biofilm. When silver ions were incorporated (Ag:HA–Lig), the anti-biofilm efficiency slightly increased (Fig. 7b).

The dynamics of *P. aeruginosa* biofilms on samples were different. The biofilm developed on the pure HA film control specimen had a gradual growth up to 72 h (Fig. 8a). The assessment of the viable cells harvested from the *P. aeruginosa* biofilms at 24 h (Fig. 8a) revealed no significant change in the number of viable cells (the

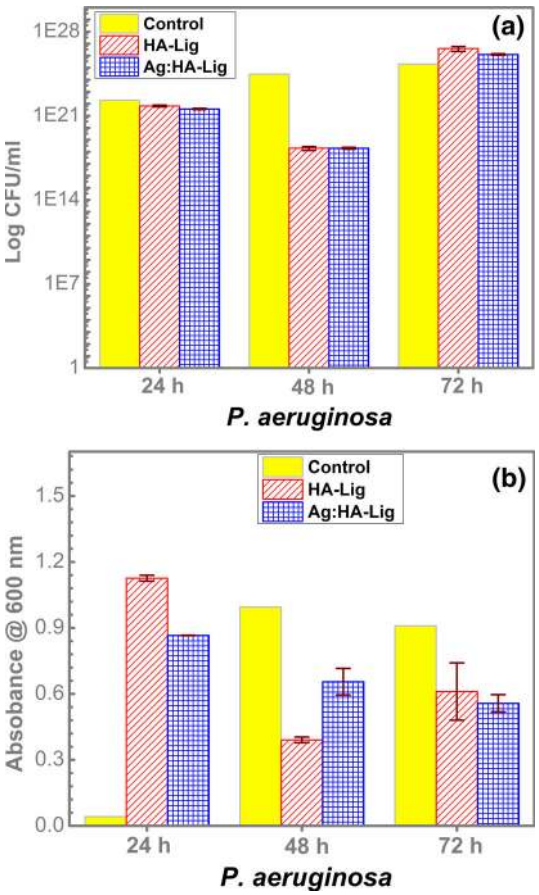

Fig. 8 (**a**) Number of *P. aeruginosa* viable cells recovered from the biofilms growing on the tested specimens after 24, 48 and 72 h, respectively; (**b**) Absorbance values at 600 nm of the *P. aeruginosa* bacterial biofilm developed on the tested specimens after 24, 48 and 72 h, respectively

quantitative difference being less than one log) developed on the HA–Lig and Ag:HA–Lig specimens, as compared to the pure HA control. Contrariwise, some interesting features were observed in the case of 48 h biofilms: both HA–Lig and Ag:HA–Lig specimens drastically decreased the number of recovered VCCs (by more than five logs) as compared to the pure HA control coating. Both MAPLE coatings showed similar bacteriostatic activity, irrespective of the presence of Ag ions. Therefore, one can suggest that the presence of Lig alone could induce increased antibacterial activity of an implant coating. All specimens showed similar antimicrobial efficiency at 72 h. The increased number of VCCs recovered at 72 h, as compared with 24 and 48 h, is pleading for the efficiency of the tested coatings to delay the biofilm development by preventing the initial microbial adherence, but not to inhibit the formation of the mature biofilm. These results could also be accounted for by the selection of a persistent bacterial population which enters in a state of metabolic latency and stop multiplying, as long as the antimicrobial substances are present, and start to multiply later, when the antimicrobial substances (in the present case Ag ions and Lig) have gone. Similar to *S. aureus* biofilms, the assessment of the total *P. aeruginosa* biofilm development (viable and dead cells) at 24 h, quantified by measuring the absorbance at 600 nm (Fig. 8b), showed that HA–Lig and Ag:HA–Lig specimens promoted the biofilm development, as compared to the pure HA control coating. However, at 48 h, a drastic decrease in the biofilm density was noticed for the composite coatings, HA–Lig being more efficient than its Ag containing counterpart. This is in good agreement with the above mentioned VCC assays, substantiating the beneficial effect of Lig on the improvement of anti-biofilm properties of the HA coatings. At 72 h, both type of organic–inorganic coatings proved equally efficient in preventing the *P. aeruginosa* biofilm cells multiplication (Fig. 8b).

VCCs assays indicated that growth of *C. famata* peaked at 72 h in the case of pure HA control coating (Fig. 9a). Irrespective of the silver ions presence, the number of viable cells recovered from the 24 and 48 h *C. famata*

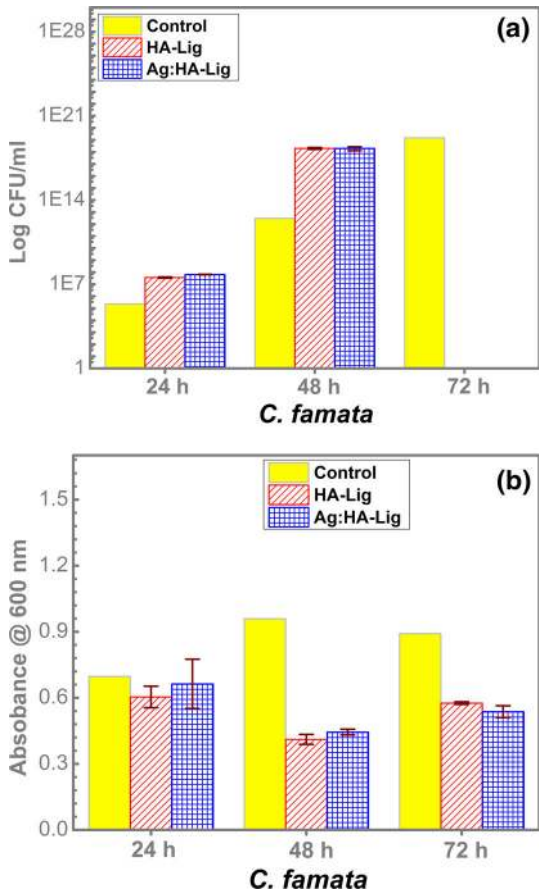

Fig. 9 (**a**) Number of *C. famata* viable cells recovered from the biofilms developed on the tested specimens after 24, 48 and 72 h, respectively; (**b**) Absorbance values at 600 nm of the *C. famata* fungal biofilm developed on the tested specimens after 24, 48 and 72 h, respectively

biofilms was higher than that obtained for the pure HA control coating, exceeding it with 2–5 logs. The HA–Lig and Ag:HA–Lig composite coatings had a strong fungicidal effect against the 72 h biofilms. These results could suggest that the HA–Lig and Ag:HA–Lig coatings induce the mature biofilm detachment from the respective surfaces. One may assume that, similar to the case of bacterial biofilms, HA–Lig itself could exhibit a large spectrum of antimicrobial activity.

The quantification of total *C. famata* biofilm by measuring the absorbance at 600 nm evidenced a clear anti-biofilm effect for the two composite coatings, which acted with similar efficiency (Fig. 9b).

Overall, the biological assays demonstrated that the organic–inorganic lignin-hydroxyapatite composite coatings synthesized by MAPLE could provide an efficient protection against microbial biofilms, without inducing any cytotoxicity towards tested WJ-MSCs.

The role of silver ions as a proficient agent against various bacterial and fungal cultures has been demonstrated [15]. It comes therefore naturally to search for alternate antimicrobial agents, which can work alone or in synergy with renowned antimicrobials.

Following the principles of antibiotic therapy, in which the risk of microbial resistance towards a drug is minimized by using antibiotherapy combinations, we propose a new approach, in which two antimicrobial substances are used to avoid the development of microbial resistance and maximize the cumulative effect. When using two antimicrobial agents, the probability of microbial resistance is the product of probabilities for resistance development used as mono-therapy (when employing singular antimicrobial agents) ($P_{1+2} = P_1 \times P_2$).

Our results reveal the potential of the natural biopolymer lignin as a reliable antimicrobial agent for implant coatings.

4 Conclusions

We report on the transfer by Matrix-Assisted Pulsed Laser Evaporation of a large macromolecule of undefined molecular weight–organosolv lignin (Lig)–embedded in a hydroxyapatite film matrix. When silver was incorporated into HA lattice, it yielded another composite, Ag:HA–Lig. The promptness and accuracy of the MAPLE technique was demonstrated for deposition of such delicate, yet bulky material, as suggested by EDS and proved by XPS and FTIR results. The obtained nanocomposites were non-cytotoxic, supporting a normal development and promoting the growth of the adhered human mesenchymal cells. The microbiological assays showed that the coated composite secured a prolonged release of silver ions, being protective both against the initial phase of microbial colonization and the mature biofilm development. The lignin addition boosted the anti-microbial activity of HA doped with silver ions against both bacterial and fungal biofilms. An implant surface modified in such a manner could host osteogenic cell proliferation while shielding from bacteria and fungi, thus facilitating a safe osteointegration of the medical device.

Acknowledgments INM, CR, NM(S), LD, AV acknowledge the support of this work by Executive Unit for Financing Higher Education, Research, Development and Innovation (*UEFISCDI*) of Romania under the ID 304/2011 and TE82/2011 contracts. GES,ACP and MAH acknowledge with thanks the financial support of TE 49/2011 research grant. AJ was financed by the FP7 Nanotech FTM Grant Agreement 245916. AJ, SE, VMS and Dj.J acknowledge with thanks financing by the Ministry of Education, Science and Technological Development, Republic of Serbia, under contract No. III 45019. All authors thank M. Enculescu for performing part of SEM investigations and G. Soricila for technical assistance in microbiological testing.

References

1. Oldani C, Dominguez A. Titanium as a biomaterial for implants. In: Fokter SK (ed) Recent Advances in Arthroplasty 2012; InTech, Rijeka. doi:10.5772/27413.
2. Juan L, Zhimin Z, Anchun M, Lei L, Jingchao Z. Deposition of silver nanoparticles on titanium surface for antibacterial effect. Int J Nanomed. 2010;5:261–7. doi:10.2147/IJN.S8810.
3. Harris LG, Richards RG. Staphylococcus aureus adhesion to different treated titanium surfaces. J Mater Sci. 2004;15:311–4. doi:10.1023/B:JMSM.0000021093.84680.bb.
4. Tang P, Zhang W, Wang Y, Zhang B, Wang H, Lin C, Zhang L. Effect of superhydrophobic surface of titanium on Staphyococcus aureus adhesion. J. Nanomater. 2011. doi:10.1155/2011/178921.
5. Høiby N, Ciofu O, Bjarnsholt T. Pseudomonas aeruginosa biofilms in cystic fibrosis. Future Microbiol. 2010;5:1663–74. doi:10.2217/fmb.10.125.
6. Tarquinio KM, Kothurkar NK, Goswami DY, Sanders RCJr, Zaritsky AL, LeVine AM. Bactericidal effects of silver plus titanium dioxide-coated endotracheal tubes on Pseudomonas aeruginosa and Staphylococcus aureus. Int J Nanomed. 2010;5:177–83. doi:10.2147/IJN.S8746.
7. Chandra J, Mukherjee PK, Leidich SD, Faddoul FF, Hoyer LL, Douglas LJ, Ghannoum MA. Antifungal resistance of candidal biofilms formed on denture acrylic in vitro. J Dent Res. 2001;80:903–8. doi:10.1177/00220345010800031101.
8. Malm A, Chudzik B, Piersiak T, Gawron A. Glass surface as potential in vitro substratum for Candida famata biofilm. Ann Agric Environ Med. 2010;17:115–8.
9. Ahariz M, Courtois P. Candida albicans biofilm on titanium: effect of peroxidase precoating. Med Devices. 2010;3:33–40. doi:10.2147/MDER.S11724.
10. Akiba N, Hayakawa I, Keh ES, Watanabe A. Antifungal effects of a tissue conditioner coating agent with TiO_2 photocatalyst. J Med Dent Sci 2005;52:223–7.
11. Arweiler-Harbeck D, Sanders A, Held M, Jerman M, Ehrich H, Jahnke K. Does metal coating improve the durability of silicone voice prostheses? Acta Oto-laryngol. 2001;121:643–6. doi:10.1080/00016480121012.
12. Surmenev RA. A review of plasma-assisted methods for calcium phosphate-based coatings fabrication. Surf Coat Technol. 2012;206:2035–56. doi:10.1016/j.surfcoat.2011.11.002.

13. Verron E, Bouler JM, Guicheux J. Controlling the biological function of calcium phosphate bone substitutes with drugs. Acta Biomater. 2012;8:3541–51. doi:10.1016/j.actbio.2012.06.022.
14. Catros S, Fricain JC, Guillotin B, Pippenger B, Bareille R, Remy M, Lebraud E, Desbat B, Amédée J, Guillemot F. Laser-assisted bioprinting for creating on-demand patterns of human osteoprogenitor cells and nano-hydroxyapatite. Biofabrication. 2011. doi:10.1088/1758-5082/3/2/025001.
15. Maillard JY, Hartemann P. Silver as an antimicrobial: facts and gaps in knowledge. Crit Rev Microbiol. 2013;39:373–83. doi:10.3109/1040841X.2012.713323.
16. Römling U, Balsalobre C. Biofilm infections, their resilience to therapy and innovative treatment strategies. J Intern Med. 2012;272:541–61. doi:10.1111/joim.12004.
17. Grainger DW, van der Mei HC, Jutte PC, van den Dungen JJ, Schultz MJ, van der Laan BF, Zaat SA, Busscher HJ. Critical factors in the translation of improved antimicrobial strategies for medical implants and devices. Biomaterials. 2013;34:9237–43. doi:10.1016/j.biomaterials.2013.08.043.
18. Schierholz JM, Morsczeck C, Brenner N, König DP, Yücel N, Korenkov M, Neugebauer E, Rump AF, Waalenkamp G, Beuth J, Pulverer G, Arens S. Special aspects of implant-associated infection in orthopedic surgery. From the pathophysiology to custom-tailored prevention strategies. Orthopade. 2004;33:397–404. doi:10.1007/s00132-004-0643-2.
19. Mijnendonckx K, Leys N, Mahillon J, Silver S, Van Houdt R. Antimicrobial silver: uses, toxicity and potential for resistance. Biometals. 2013;26:609–21. doi:10.1007/s10534-013-9645-z.
20. Cazacu G, Capraru M, Popa VI. Advances concerning Lignin utilization in new materials. In: Thomas S, Visak PM, Mathew AP (eds). Advances in Natural Polymers: Composites and Nanocomposites. New York, Heidelberg: Springer; 2013. p. 255–312.
21. Eraković S, Janković A, Veljović Dj, Palcevskis E, Mitrić M, Stevanovic T, Janaćković Dj, Mišković-Stanković V. Corrosion stability and bioactivity in simulated body fluid of silver/hydroxyapatite and silver/hydroxyapatite/lignin coatings on titanium obtained by electrophoretic deposition. J Phys Chem B. 2013;117:1633–43. doi:10.1021/jp305252a.
22. Eraković S, Veljović Dj, Diouf PN, Stevanović T, Mitrić M, Janaćković Dj, Matić IZ, Juranić ZD, Mišković-Stanković V. Investigation of silver impact on hydroxyapatite/lignin coatings electrodeposited on titanium. Prog Org Coat. 2012;75:275–83. doi:10.1016/j.porgcoat.2012.07.005.
23. Santillán MJ, Quaranta NE, Boccaccini AR. Titania and titania–silver nanocomposite coatings grown by electrophoretic deposition from aqueous suspensions. Surf Coat Technol. 2010;205:2562–71. doi:10.1016/j.surfcoat.2010.10.001.
24. Pique A. Deposition of polymers and biomaterials using the Matrix-Assisted Pulsed Evaporation (MAPLE) process. In: R Eason (ed). Pulsed Laser Deposition of Thin Films. Applications-Led Growth of Functional Materials. New Jersey: Wiley Interscience; 2007. p. 63–84.
25. Cristescu R, Popescu C, Popescu AC, Grigorescu S, Duta L, Mihailescu IN, Caraene G, Albulescu R, Albulescu L, Andronie A, Stamatin I, Ionescu A, Mihaiescu D, Buruiana T, Chrisey DB. Functionalized polyvinyl alcohol derivatives thin films for controlled drug release and targeting systems: mAPLE deposition and morphological, chemical and in vitro characterization. Appl Surf Sci. 2009;255:5600–4. doi:10.1016/j.apsusc.2008.09.047.
26. Cristescu R, Popescu C, Popescu AC, Grigorescu S, Duta L, Mihailescu IN, Andronie A, Stamatin I, Ionescu OS, Mihaiescu D, Buruiana T, Chrisey DB. Laser processing of polyethylene glycol derivative and block copolymer thin films. Appl Surf Sci. 2009;255:5605–10. doi:10.1016/j.apsusc.2008.09.060.
27. Miroiu FM, Socol G, Visan A, Stefan N, Craciun D, Craciun V, Dorcioman G, Mihailescu IN, Sima LE, Petrescu SM, Andronie A, Stamatin I, Moga S, Ducu C. Composite biocompatible hydroxyapatite–silk fibroin coatings for medical implants obtained by Matrix Assisted Pulsed Laser Evaporation. Mater Sci Eng. 2010;169:151–8. doi:10.1016/j.mseb.2009.10.004.
28. Cristescu R, Popescu C, Socol G, Visan A, Mihailescu IN, Gittard SD, Miller PR, Martin TN, Narayan RJ, Andronie A, Stamatin I, Chrisey DB. Deposition of antibacterial of poly(1,3-bis-(p-carboxyphenoxy propane)-co-(sebacic anhydride)) 20:80/gentamicin sulfate composite coatings by MAPLE. Appl Surf Sci. 2011;257:5287–92. doi:10.1016/j.apsusc.2010.11.141.
29. Sygnatowicz M, Tiwari A. Controlled synthesis of hydroxyapatite-based coatings for biomedical application. Mater Sci Eng. 2009;29:1071–6. doi:10.1016/j.msec.2008.08.036.
30. Eraković S, Janković A, Ristoscu C, Duta L, Serban N, Visan A, Mihailescu IN, Stan GE, Socol M, Iordache O, Dumitrescu I, Luculescu CR, Janaćković Dj, Mišković-Stanković V. Antifungal activity of Ag:hydroxyapatite thin films synthesized by pulsed laser deposition on Ti and Ti modified by TiO_2 nanotubes substrates. Appl Surf Sci. 2014;293:37–45. doi:10.1016/j.apsusc.2013.12.029.
31. Grumezescu AM, Andronescu E, Ficai A, Bleotu C, Chifiriuc MC. Chitin based biomaterial for antimicrobial therapy: fabrication, characterization and in vitro profile based interaction with eukaryotic and prokaeryotic cells. Biointerface Res Appl Chem 2012; 5:438–45.
32. Cros A. Charging effects in X-ray photoelectron spectroscopy. J Electron Spectrosc Relat Phenom. 1992;59:1–14. doi:10.1016/0368-2048(92)85008-U.
33. Johansson LS, Campbell JM. Reproducible XPS on biopolymers: cellulose studies. Surf Interface Anal. 2004;36:1018–22. doi:10.1002/sia.1827.
34. Guo JB, Tao ZY, Luo XG. Analysis of bamboo lignin with FTIR and XPS. Acta Chim. Sin. 2005; 63:1536–40.
35. Kalaskar DM, Ulijn RV, Gough JE, Alexander MR, Scurr DJ, Sampson WW, Eichhorn SJ. Characterisation of amino acid modified cellulose surfaces using ToF-SIMS and XPS. Cellulose. 2010;17:747–56. doi:10.1007/s10570-010-9413-y.
36. http://en.wikipedia.org/wiki/Lignin. Accessed 28 Jan 2014.
37. Markovic M, Fowler BO, Tung MS. Preparation and comprehensive characterization of a calcium hydroxyapatite reference material. J Res Natl Inst Stand Technol. 2004;109:553–68. doi:10.6028/jres.109.042.
38. Guo GS, He CN, Wang ZH, Gu FB, Han DM. Synthesis of titania and titanate nanomaterials and their application in environmental analytical chemistry. Talanta. 2007;72:1687–92. doi:10.1016/j.talanta.2007.03.039.
39. Kline LM, Hayes DG, Womac AR, Labbé N. Simplified determination of lignin content in hard and soft woods via UV-spectrophotometric analysis of biomass dissolved in ionic liquids. BioResources. 2010; 5:1366–1383.
40. Rana R, Langenfeld-Heyser R, Finkeldey R, Polle A. FTIR spectroscopy, chemical and histochemical characterisation of wood and lignin of five tropical timber wood species of the family of Dipterocarpaceae. Wood Sci Technol. 2010;44:225–42. doi:10.1007/s00226-009-0281-2.
41. Popescu CM, Popescu MC, Singurel G, Vasile C, Argyropoulos DS, Willfor S. Spectral characterization of eucalyptus wood. Appl Spectrosc. 2007;61:1168–77. doi:10.1366/000370207782597076.
42. Fan M, Dai D, Huang B. Fourier transform infrared spectroscopy for natural fibres. In: S Salih, editor. Fourier Transform–Materials Analysis. 2012, InTech; p. 45–68.
43. Hergert HL. Infrared spectra of lignin and related compounds. II. Conifer lignin and model compounds. J Org Chem. 1960;25:405–13. doi:10.1021/jo01073a026.
44. Tejado A, Peña C, Labidi J, Echeverria JM, Mondragon I. Physico-chemical characterization of lignins from different

sources for use in phenol-formaldehyde resin synthesis. Bioresour Technol. 2007;98:1655–63. doi:10.1016/j.biortech.2006.05.042.
45. Grumezescu AM, Holban AM, Andronescu E, Mogosanu GD, Vasile BS, Chifiriuc MC, Lazar V, Andrei E, Constantinescu A, Maniu H. Anionic polymers and 10 nm Fe_3O_4@UA wound dressings support human foetal stem cells normal development and exhibit great antimicrobial properties. Int J Pharm. 2013. doi:10.1016/j.ijpharm.2013.08.026.
46. Bianco P, Riminucci M, Gronthos S, Robey PG. Bone marrow stromal stem cells: nature, biology, and potential applications. Stem Cells. 2001;19:180–92. doi:10.1634/stemcells.19-3-180.
47. Forte G, Franzese O, Pagliari S, Pagliari F, Di Francesco AM, Cossa P, Laudisi A, Fiaccavento R, Minieri M, Bonmassar E, Di Nardo P. Interfacing Sca-1^{pos} mesenchymal stem cells with biocompatible scaffolds with different chemical composition and geometry. J Biomed Biotechnol. 2009. doi:10.1155/2009/910610.
48. Zhao L, Chu PK, Zhang Y, Wu Z. Antibacterial coatings on titanium implants. J Biomed Mater Res B. 2009;91:470–80. doi:10.1002/jbm.b.31463.
49. Schmidmaier G, Lucke M, Wildemann B, Haas NP, Raschke M. Prophylaxis and treatment of implant-related infections by antibiotic-coated implants: a review. Injury. 2006;37:S105–12. doi:10.1016/j.injury.2006.04.016.
50. Agnihotri S, Mukherji S, Mukherji S. Immobilized silver nanoparticles enhance contact killing and show highest efficacy: elucidation of the mechanism of bactericidal action of silver. Nanoscale. 2013;5:7328–40. doi:10.1039/C3NR00024A.
51. Arumugam SK, Sastry TP, Sreedhar B, Mandal AB. One step synthesis of silver nanorods by autoreduction of aqueous silver ions with hydroxyapatite: an inorganic–inorganic hybrid nanocomposite. J Biomed Mater Res. 2007;80:391–8. doi:10.1002/jbm.a.30895.